Two-stage Framework for Microgrids Energy Management Considering Demand Response Program and Compressed Air Energy Storages under Uncertainties

Alireza Azarhooshang [1], Sasan Pirouzi [2*], Mojtaba Ghadamyari[1]

[1] Department of Electrical Engineering, Shahid Beheshti University, Tehran, Iran, (a.azarhooshang@gmail.com, ghadamyari.mij@gmail.com)
[2]Power System Group, Semirom Branch, Islamic Azad University, Semirom, Iran, s.pirouzi@sutech.ac.ir

Abstract

This paper presents a two-stage stochastic model for the management of microgrids. In the proposed model, the uncertainties related to the generation output of wind turbines, the consumption load, and the electrical energy price have been taken into account. The presented two-stage problem is modeled as a mixed-integer linear programming (MILP) problem and solved by the CPLEX solver of the GAMS software. In the first stage, the operation areas of individual microgrids are determined. To this end, the considered model is implemented on the 118-bus IEEE distribution system and the security constraints of the distribution system are considered. In the second stage, the microgrid operation problem is solved considering the microgrids' operation area. The second stage is solved as single-objective and multi-objective problems separately. Objective functions in the multi-objective case include the operating costs and the amount of pollutant emissions. The results show that an increase in the operating costs due to the reduction in the amount of emissions in the bi-objective case. It is worth noting that the multi-objective model provided in this study is solved using the fuzzy and the ε-constraint methods separately. The comparison indicates a more reduction in the operating costs in the ε -constraint method than the fuzzy method. However, the reduction of emissions in the fuzzy method is higher than that of the ε-constraint method. Further, more investigations prove the effectiveness of the DRP on the correction of the demand curve and the reduction in the operating costs.

Keywords: Multi-Objective Energy Management, Islanded Microgrids, Emission, Demand Response Program, Compressed Air Energy Storage.
Article history: Received 26-Aug-2021; Revised …-…-2021; Accepted …-…-2021.

* Corresponding Author: **S. Pirouzi**, e-mail: s.pirouzi@sutech.ac.ir

1. Introduction

A) Motivation and Literature Review

Natural disasters such as earthquakes, hurricanes, and floods have increased in recent years due to climate change. Due to the direct or indirect impact of these events on the power system, concepts such as reliability and security have been addressed in particular in power system research in recent years. The reason is that these concepts are closely related to both social welfare and economic issues. In this regard, to enhance the flexibility and reliability of power systems, the resilience problem has been extensively studied and some new indices have been developed for this purpose [1]. To study the concept of resilience and its dimensions in distribution networks, the idea of utilizing smart grid technologies as an effective tool to enhance resilience of distribution networks has been presented in [2] in such a way that the possibility of an islanded operation for critical conditions is investigated and appropriate indices are introduced for this purpose, including checking the number of disconnected lines due to a fault and system restoration after the fault occurrence.

The development process in this context is examined in [3] and the necessary infrastructure necessary for the generation, transmission, distribution, and consumption sectors is described. In the present study, the overall objectives of the R&D project are as follows: (a) Modernizing the distribution network, using advanced technologies, and creating operational examples, and (b) Supporting the increases capacity of renewable

energy sources (RESs) and maintaining the reliability and resiliency. In [4], a conceptual approach is presented for making changes to achieve a flexible distribution system through microgrids. In this study, three operational examples of the concept of resiliency enhancement are mentioned and their practical results are presented. The results show that communities can operate power systems in modern distribution systems without losing operational capability in the event of a fault and also quickly return to the normal mode under normal operation conditions.

In [5] discusses the role of microgrids as distributed power systems to increase system reliability in the event of severe events. The study suggests that the use of microgrids will allow large networks to increase system resilience more than smaller networks and be more robust against fluctuations. In [6] discusses the strategies and smart grid technologies as a tool to increase system resilience by emphasizing new technologies such as topology reconfiguration of the network, microgrids, and distribution automation. To illustrate how to increase system resilience against extreme events, this paper proposes a load restoration method based on smart distribution technology. In [7], a decision framework is designed to modernize the network and improve system performance in restoration operations under severe climatic conditions. Benefits of using the proposed framework include optimizing the allocation of resources and repairs crews, improving the restoration process, and reducing customer interruption time. In addition, recent studies have addressed the resilience measurement problem in the distribution network. The authors in [8] present a new method for measuring the resilience of a distribution system; the aim of this study is to measure resilience for some of the existing proposals and compare different methods as far as possible. In [9], the evaluation of distribution system resilience is modeled as a multi-criteria decision making problem and the resilience is computed using the Graphs Theory. However, the methods presented in this study mainly focus on characteristics of the configuration structure of distribution networks and may not adequately represent the electrical properties, available capacities, and nature of events in this segment of the power system. In [10] presents a service restoration process that uses free-generation capacity microgrids to supply critical loads in distribution feeders after a severe event. The main objective of this study was to determine the feasibility of using microgrids for critical load restoration.

The problem of optimizing the support service in smart distribution networks is discussed in [11]. This study explores what the frequency reduction settings of distributed generation resources (DGs) should be for maximum load restoration. In [12], the problem of optimal planning for energy management in microgrids is investigated. The objective function considered in this study is to minimize net operating costs considering the uncertainty of RESs. However, the possibility of occurrence of severe events is not taken into account. In [13] provides an effective approach for flexible planning of static microgrids. Nevertheless, the geographical conditions of the distribution network and its limitations have yet to be investigated. In [14], the subject of microgrid establishment in dynamic distribution networks is discussed from the perspective of energy management and optimal utilization of RESs. A new structure of microgrids is proposed in [15] to simplify its optimal planning, and DRPs are implemented to reduce customers' costs. A new framework for daily planning of smart distribution networks based on robust optimization approach is presented in in [16] to secure system performance against worst-case scenario of variables with uncertainty. However, the occurrence of severe events has not been addressed in the above studies.

B) Contributions

In this paper, a multi-objective stochastic model is presented for determining the service area of microgrids and solving the energy management problem of microgrids in distribution networks. The notable points of the proposed model are provided as follows:

- Solving the problem considering the network security constraints in both grid-connected and islanded modes to accurately determine the operation area of individual microgrids,
- Investigating the impact of using a DRP on the consumption patterns and operating costs,
- Using compressed-air energy storage (CAES) system instead of battery-based storage systems (BBSSs) thanks to their longer service life, and
- Solving the considered problem in both single-objective and multi-objective ways to study the influence of each method on operating costs and emission rates.

C) Paper Organization

The remainder of the paper is organized as follows. Section 2 outlines the proposed model. Section 3 presents the mathematical model used. In Section 4, the flowchart of the proposed model is described. The results of implementation of the proposed model on the 118-bus IEEE network are also analyzed in Section 5. Finally, conclusions are provided in Section 6.

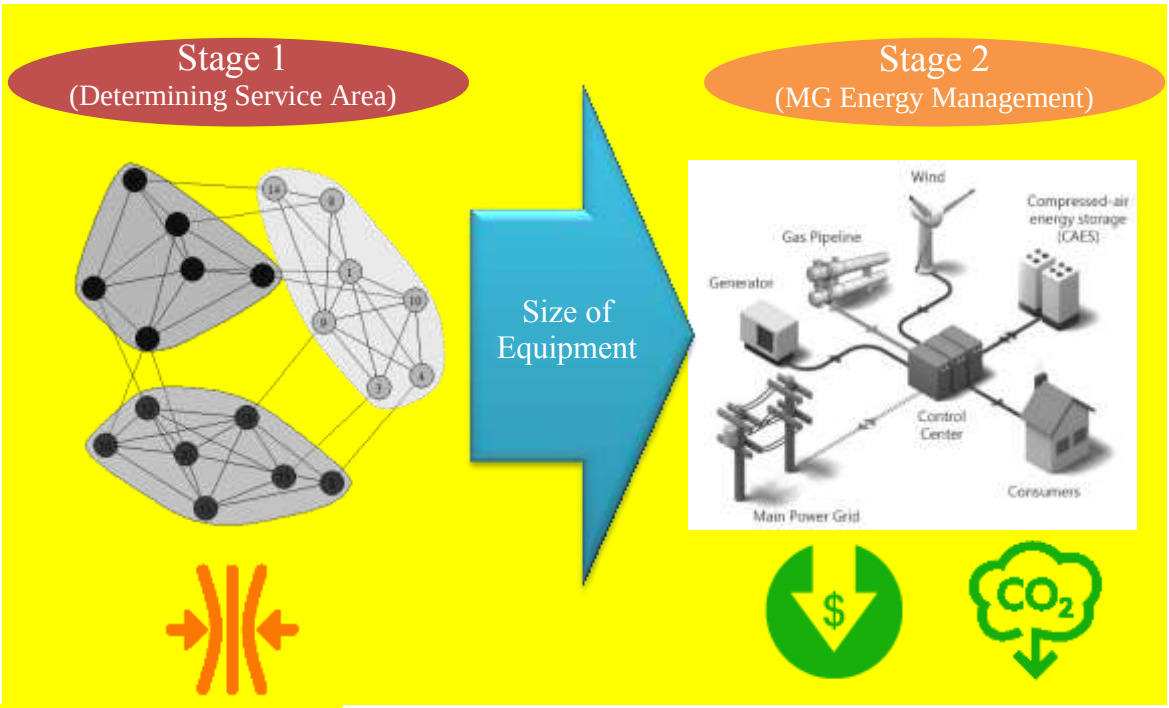

Fig. 1. The layout of the proposed model

2. Model of the Proposed Scheme

Fig. 1 illustrates the layout of the proposed model. The model consists of two main stages. The first stage is relating to determining the operation area of each microgrid in which the complete specifications of the network including power flow, line capacity, voltage limitations, and operation of various equipment are taken into account. The primary purpose of the first stage is to specify the configuration of each microgrid in order to supply as much demand as possible. The main goal of the second stage is to minimize the operating cost and emission level. In this stage, the capacity of the operation equipment is determined according to the controllable area of each microgrid.

A) Formulation of the First Stage

In the first stage, with regard to the objective of supplying the maximum demand as possible under special conditions, such as fault occurrence and/or planned attacks, the objective function of interest to determine the controllable area of microgrids is given in (1) [17]:

$$\max:\ \text{Recovery} = \frac{\sum_{t\in T}\sum_{i\in I}(\text{Pr}_{i,t}^{L}\times\sum_{s\in S}\rho_s P_{i,t,s}^{L})}{\sum_{t\in T}\sum_{i\in I}(\text{Pr}_{i,t}^{L}\times\sum_{s\in S}\rho_s P_{i,t,s}^{Load})} \quad (1)$$

where $\text{Pr}_{i,t}^{L}$ is the importance factor of the load, $P_{i,t,s}^{L}$ denotes the load supplied at each bus, and ρ_s shows the occurrence probability of each scenario. In the above function, the supplied load level is specified according to the importance of the load. It is clear that the final operation area of the microgrids is determined so that maximum important loads are supplied.

B) Determining Service Area Formulation

The Graph Theory is used in this study to apply the planning constraints to the formation of the area of microgrids, where a binary variable is used to show the activation status of each of the lines and/or buses of the network. Equations (2) to (8) give the constraints related to the determination of the network graph. Equation (2) expresses the condition of each bus possessed by only one single microgrid. Furthermore, Eq. (3) states that the rest of the buses can be possessed by a microgrid only if the root bus of that microgrid is active. It is worth noting that the root bus of a microgrid is a bus with the master generator [18].

$$\sum_{k=1}^{N_{MGs}}\alpha_{i,k}\le 1 \quad (2)$$

$$\alpha_{i,k}\le\alpha_{r,k} \quad (3)$$

To ensure the continuity of the formed graph, Eq. (4) states the constraint related to the links to other buses of each microgrid. In other words, if a bus is possessed by a microgrid, one of the neighbors of the bus should also belong to that microgrid.

$$\alpha_{i,k}\le\sum_{\forall j\in\xi_i}\alpha_{j,k} \quad (4)$$

Equation (5) denotes the connection between two binary variables related to the lines and buses of the network. As is seen, the operation of a line is

possible only of both the near and end buses of the line belong to the same microgrid. Moreover, to make it possible to schedule buses out of the planning, i.e. buses without any faults or interruptions, the logic term $\odot$ is used as such that in case the near and end buses do not belong to any of the microgrids the line can still be operated.

$$B_l \le \alpha_{i,k} \odot \alpha_{j,k} \tag{5}$$

To linearize Eq. (5), Eqs. (6) to (8) are employed:

$$B_l \le \chi_{l,k} + \chi'_{l,k} \tag{6}$$

$$\begin{cases} \chi_{l,k} \le \alpha_{i,k} \\ \chi_{l,k} \le \alpha_{j,k} \\ \chi_{l,k} \ge \alpha_{i,k} + \alpha_{j,k} - 1 \end{cases} \tag{7}$$

$$\begin{cases} \chi'_{l,k} \le 1 - \alpha_{i,k} \\ \chi'_{l,k} \le 1 - \alpha_{j,k} \\ \chi'_{l,k} \ge 1 - \alpha_{i,k} - \alpha_{j,k} \end{cases} \tag{8}$$

In Eqs. (9) and (10), the amount of load supplied at individual buses is calculated based on the binary variables of the formed graph. In these equations, $P_{i,t,s}^{Load}$ and $Q_{i,t,s}^{Load}$ respectively show the predicted load levels for active and reactive powers at each scenario.

$$P_{i,t,s}^{L} = \sum_{k \in K} \alpha_{i,k} P_{i,t,s}^{Load} - P_{i,t,s}^{LC} \tag{9}$$

$$Q_{i,t,s}^{L} = \sum_{k \in K} \alpha_{i,k} Q_{i,t,s}^{Load} - \tan(\varphi_i) P_{i,t,s}^{LC} \tag{10}$$

In Eq. (9), $P_{i,t,s}^{LC}$ exhibits the amount of use of the load control. How to calculate and determine the range of this variable is shown in Eqs. (11) to (13). Also, how to use load control for resiliency is in the form of a stagewise function, where large loads at each point can curtail part of their loads at a specific number of stages.

$$P_{i,t,s}^{LC} \le \sum_{k \in K} \alpha_{i,k} P_{i,t}^{LC,Max} \tag{11}$$

$$P_{i,t,s}^{LC} \le \sum_{d \in D} \sigma_{i,d,t,s}^{LC} P_{i,d,t}^{Curt} \tag{12}$$

$$\sum_{d \in D} \sigma_{i,d,t,s}^{LC} \le 1 \tag{13}$$

The limitation on the utilization of power plants at each microgrid is determined in (14) and (15) based on the possession binary variable of the bus. Also, the reactive power generation or consumption ranges are modeled in (16) and (17).

$$P_{g,t,s}^{DG} \le P_g^{DG,Max} \sum_{i \in I_g} \sum_{k \in K} \alpha_{i,k} \tag{14}$$

$$P_{g,t,s}^{DG} \ge P_g^{DG,Min} \sum_{i \in I_g} \sum_{k \in K} \alpha_{i,k} \tag{15}$$

$$Q_{g,t,s}^{DG} \le Q_g^{DG,Max} \sum_{i \in I_g} \sum_{k \in K} \alpha_{i,k} \tag{16}$$

$$Q_{g,t,s}^{DG} \ge Q_g^{DG,Min} \sum_{i \in I_g} \sum_{k \in K} \alpha_{i,k} \tag{17}$$

Equations (18) to (25) show how the CAES system is modeled [19]. With regard to pressure changes of the tank air in the operation of the CAES system, Eqs. (18) and (19) express the link between the pressure changes and the generation/consumption power. Further, Eqs. (20) to (22) provide the operation limitations of the storage system. To calculate the tank pressure during different hours considering operation limitations, Eqs. (23) to (25) are employed.

$$A_{es,t,s}^{Inject} = \alpha^{Inject} P_{es,t,s}^{Ch} \tag{18}$$

$$A_{es,t,s}^{Pump} \alpha^{Pump} = P_{es,t,s}^{Dis} \tag{19}$$

$$A_{es}^{Inject,Min} I_{es,t,s}^{Ch} \le A_{es,t,s}^{Inject} \le A_{es}^{Inject,Max} I_{es,t,s}^{Ch} \tag{20}$$

$$A_{es}^{Pump,Min} I_{es,t,s}^{Dis} \le A_{es,t,s}^{Pump} \le A_{es}^{Pump,Max} I_{es,t,s}^{Dis} \tag{21}$$

$$0 \le I_{es,t,s}^{Ch} + I_{es,t,s}^{Dis} \le \sum_{i \in I_{es}} \sum_{k \in K} \alpha_{i,k} \tag{22}$$

$$PS_{es,t,s} = PS_{es,t-1,s} + (A_{es,t,s}^{Inject} - A_{es,t,s}^{Pump}) dt \tag{23}$$

$$PS_{es}^{Min} \le PS_{es,t,s} \le PS_{es}^{Max} \tag{24}$$

$$PS_{es,T,s} = PS_{es,0,s} \tag{25}$$

Regarding the influence of renewable wind power plants in the grid, Eq. (26) calculates the amount of produced energy concerning the wind speed [20]:

$$P_{w,t,s}^{Wind} = \begin{cases} 0 & v_{w,t,s} \le v_{ci}, v_{w,t,s} \ge v_{co} \\ p_r \dfrac{v_{w,t,s} - v_{ci}}{v_r - v_{ci}} & v_{ci} \le v_{w,t,s} \le v_r \\ p_r & v_r \le v_{w,t,s} \le v_{co} \end{cases} \tag{26}$$

Equations (27) to (34) indicate the power balance equation and how the transmission lines are operated. Equations (27) and (28) respectively show the active and reactive power balance. A linear model available in [21] is used to solve the power flow problem. The power flow equations are presented in (29) to (34).

$$\sum_{g \in G_i} P_{g,t,s}^{DG} + \sum_{es \in ES_i} P_{es,t,s}^{Dis} + \sum_{w \in W_i} P_{w,t,s}^{Wind} + \sum_{l \in L_i^t} P_{l,t,s}^{Flow} = P_{i,t,s}^{L} + \sum_{es \in ES_i} P_{es,t,s}^{Ch} + \sum_{l \in L_i^f} P_{l,t,s}^{Flow} \tag{27}$$

$$\sum_{g \in G_i} Q_{g,t,s}^{DG} + \sum_{l \in L_i^t} Q_{l,t,s}^{Flow} = Q_{i,t,s}^{L} + \sum_{l \in L_i^f} Q_{l,t,s}^{Flow} \tag{28}$$

$$k^1{}_l = \frac{r_l}{r_l^2 + x_l^2}, \quad k^2{}_l = \frac{x_l}{r_l^2 + x_l^2} \tag{29}$$

$$P_{l,t,s}^{Flow} = k^1{}_l \left(V_{i,t,s} - V_{j,t,s} \right) + k^2{}_l \left(\delta_{i,t,s} - \delta_{j,t,s} \right) \tag{30}$$

$$Q_{l,t,s}^{Flow} = k^1{}_l \left(\delta_{j,t,s} - \delta_{i,t,s} \right) + k^2{}_l \left(V_{i,t,s} - V_{j,t,s} \right) \tag{31}$$

$$-Q_{l,t,s}^{Flow,Max} B_l \le Q_{l,t,s}^{Flow} \le Q_{l,t,s}^{Flow,Max} B_l \tag{32}$$

$$-P_{l,t,s}^{Flow,Max} B_l \le P_{l,t,s}^{Flow} \le P_{l,t,s}^{Flow,Max} B_l \quad (33)$$

$$V_i^{Min} \le V_{i,t,s} \le V_i^{Max} \quad (34)$$

C) Formulation of the Second Stage

In the second stage, the cost and emission functions are considered to solve the energy management problem. These functions are given in (35) and (36), respectively [22,23]:

$$\min: \text{Cost} = \sum_{s\in S}\rho_s \sum_{t\in T}\sum_{k\in K}\begin{Bmatrix} a_k + b_k P_{k,t,s}^{DG} + c_k P_{k,t,s}^{DG\,2} \\ +\left|d_k \sin\left(e_k\left(P_k^{DG,Min} - P_{k,t,s}^{DG}\right)\right)\right| \\ +C_k^{SU} u_{k,t,s}^{SU} + C_k^{SD} u_{k,t,s}^{SD} \\ +C_{k,t,s}^{LC} + C_{k,t,s}^{M} + C_{k,t,s}^{ES} \end{Bmatrix} \quad (35)$$

$$\min: \text{Emission} = \sum_{s\in S}\rho_s \sum_{t\in T}\sum_{k\in K}\begin{Bmatrix} 10^{-2}\left(\alpha_k + \beta_k P_{k,t,s}^{G} + \gamma_k P_{k,t,s}^{G\,2}\right) \\ +\varsigma_k \exp(\lambda_k P_{k,t,s}^{G}) + E_{k,t,s}^{ES} \end{Bmatrix} \quad (36)$$

Equations (35) consists of four main terms, including the costs of power plants, load control, and power exchange with the grid and the cost of the storage system. The cost of a power plant in this study comprises of the fuel cost function and the start up/shut down cost. Additionally, Eq. (36) calculates the pollution level emitted by power plants and the gas consumption by the storage system.

According to the goal of the paper to investigate the operation conditions under both single- and bi-objective cases, the objective function of the single-objective model is shown in Eq. (37). In this equation, the total system cost is calculated by adding the emission cost to the operating cost.

$$\min: \text{Total Cost} = \text{Cost} + \lambda^{EM}\,\text{Emission} \quad (37)$$

D) Energy Management in Microgrids

Equations (38) to (44) illustrate the operation of power plants in the grid. The operation limit of power plants is given in Eqs. (38) to (40). To limit the amount of power variations at successive hours, we use Eqs. (41) and (42). According to the inclusion of the start up and shut down cost in the objective function, Eqs. (43) and (44) are utilized to identify the start up and shut down times.

$$P_k^{DG,Min} = \sum_{g\in G} P_g^{DG,Min} \sum_{i\in I_g} \alpha_{i,k} \quad (38)$$

$$P_k^{DG,Max} = \sum_{g\in G} P_g^{DG,Max} \sum_{i\in I_g} \alpha_{i,k} \quad (39)$$

$$P_k^{DG,Min} u_{k,t,s}^{DG} \le P_{k,t,s}^{DG} \le PD_k^{G,Max} u_{k,t,s}^{DG} \quad (40)$$

$$P_{k,t,s}^{DG} - P_{k,t-1,s}^{DG} \le P_k^{RU} + P_k^{DG,Min} u_{k,t,s}^{SU} \quad (41)$$

$$P_{k,t-1,s}^{DG} - P_{k,t,s}^{DG} \le P_k^{RD} + P_k^{DG,Min} u_{k,t,s}^{SD} \quad (42)$$

$$u_{k,t,s}^{SU} - u_{k,t,s}^{SD} = u_{k,t,s}^{DG} - u_{k,t-1,s}^{DG} \quad (43)$$

$$u_{k,t,s}^{SU} + u_{k,t,s}^{SD} \le 1 \quad (44)$$

Equations (45) to (50) show how the power is exchanged with the grid. Also, Eqs. (45) to (48) express the capacity limit of power exchange with the main grid for both directions. The asynchronous purchase and sale constraint is also modeled in Eq. (49). Equation (50) calculates the cost or revenue as the result of the power exchange with the main grid.

$$-P_k^{M,Max} \le P_{k,t,s}^{M} \le P_k^{M,Max} \quad (45)$$

$$P_{k,t,s}^{M} = P_{k,t,s}^{M,Sell} - P_{k,t,s}^{M,Buy} \quad (46)$$

$$0 \le P_{k,t,s}^{M,Sell} \le P_k^{M,Max} \times u_{k,t,s}^{Sell} \quad (47)$$

$$0 \le P_{k,t,s}^{M,Buy} \le P_k^{M,Max} \times u_{k,t,s}^{Buy} \quad (48)$$

$$u_{k,t,s}^{Sell} + u_{k,t,s}^{Buy} \le 1 \quad (49)$$

$$C_{k,t,s}^{M} = \rho_{t,s}^{Power} \times P_{k,t,s}^{M} \quad (50)$$

Regarding that the capacity of the storage system is determined, Eqs. (51) to (67) model the operation of the CAES system. Also, Eqs. (51) to (56) specify the equipment capacity based on the configuration of the microgrid. The operation and calculation of charging and discharging of the storage system considering the tank pressure changes are presented in Eqs. (57) to (61). Equations (62) to (64) consider the pressure level and minimum and maximum limits of the tank pressure. Moreover, the amount of consumed gas when the storage system produces power is shown in Eq. (65). The cost and emissions imposed by the storage system are respectively calculated in Eqs. (66) and (67).

$$A_k^{Inject,Min} = \sum_{es\in ES} A_{es}^{Inject,Min} \sum_{i\in I_{es}} \alpha_{i,k} \quad (51)$$

$$A_k^{Inject,Max} = \sum_{es\in ES} A_{es}^{Inject,Max} \sum_{i\in I_{es}} \alpha_{i,k} \quad (52)$$

$$A_k^{Pump,Min} = \sum_{es\in ES} A_{es}^{Pump,Min} \sum_{i\in I_{es}} \alpha_{i,k} \quad (53)$$

$$A_k^{Pump,Max} = \sum_{es\in ES} A_{es}^{Pump,Max} \sum_{i\in I_{es}} \alpha_{i,k} \quad (54)$$

$$PS_k^{Min} = \sum_{es\in ES} PS_{es}^{Min} \sum_{i\in I_{es}} \alpha_{i,k} \quad (55)$$

$$PS_k^{Max} = \sum_{es\in ES} PS_{es}^{Max} \sum_{i\in I_{es}} \alpha_{i,k} \quad (56)$$

$$A_{k,t,s}^{Inject} = \alpha^{Inject} P_{k,t,s}^{Ch} \quad (57)$$

$$A_{k,t,s}^{Pump} \alpha^{Pump} = P_{k,t,s}^{Dis} \quad (58)$$

$$A_k^{Inject,Min} I_{k,t,s}^{Ch} \le A_{k,t,s}^{Inject} \le A_k^{Inject,Max} I_{k,t,s}^{Ch} \quad (59)$$

$$A_k^{Pump,Min} I_{k,t,s}^{Dis} \le A_{k,t,s}^{Pump} \le A_k^{Pump,Max} I_{k,t,s}^{Dis} \quad (60)$$

$$0 \le I_{k,t,s}^{Ch} + I_{k,t,s}^{Dis} \le 1 \quad (61)$$

$$PS_{k,t,s} = PS_{k,t-1,s} + (A_{k,t,s}^{Inject} - A_{k,t,s}^{Pump})dt \quad (62)$$

$$PS_k^{Min} \le PS_{k,t,s} \le PS_k^{Max} \quad (63)$$

$$PS_{k,T,s} = PS_{k,0,s} \quad (64)$$

$$P_{k,t,s}^{Gas} = \alpha^{HR} P_{k,t,s}^{Dis} \quad (65)$$

$$C_{k,t,s}^{EC} = \rho_t^{Gas} P_{k,t,s}^{Gas} \quad (66)$$

$$E_{k,t,s}^{ES} = EM_k^{Net,Gas} P_{k,t,s}^{Gas} \quad (67)$$

By considering the shiftable-load DRP, the constraints related to the DRP are presented in Eqs. (68) to (74). Equations (68) to (70) specify the acceptable limit of use of load shifting for increasing or decreasing the load. Equation (71) models the asynchronous constraint of the load increase or decrease at each hour. Also, Eq. (72) shows that the amount of reduction in the load should be equal to that of the increase in the load during the 24-hour planning horizon. The cost of use of load shifting and the amount of load after shifting are calculated in Eqs. (73) and (74), respectively.

$$P_{k,t,s}^{LC,Max} = \sum_{i \in I} P_{i,t,s}^{LC} \alpha_{i,k} \quad (68)$$

$$P_{k,t,s}^{LC,Do} \le P_{k,t,s}^{LC,Max} I_{k,t,s}^{Do} \quad (69)$$

$$P_{k,t,s}^{LC,Up} \le P_{k,t,s}^{LC,Max} I_{k,t,s}^{Up} \quad (70)$$

$$0 \le I_{k,t,s}^{Up} + I_{k,t,s}^{Do} \le 1 \quad (71)$$

$$\sum_{t \in T} P_{k,t,s}^{LC,Do} = \sum_{t \in T} P_{k,t,s}^{LC,Up} \quad (72)$$

$$C_{k,t,s}^{LC} = a_k^{LC} (I_{k,t,s}^{Up} + I_{k,t,s}^{Do}) + b_k^{LC} (P_{k,t,s}^{LC,Up} + P_{k,t,s}^{LC,Do}) \quad (73)$$

$$P_{k,t,s}^{Load} = \sum_{i \in I} P_{i,t,s}^{Load} \alpha_{i,k} - P_{k,t,s}^{LC,Do} + P_{k,t,s}^{LC,Up} \quad (74)$$

Based on the hourly load curve at each microgrid and the available equipment, the power balance equation for each microgrid is written in Eq. (75).

$$P_{k,t,s}^{DG} + P_{k,t,s}^{Dis} + P_{k,t,s}^{M,Buy} = P_{k,t,s}^{Load} + P_{k,t,s}^{Ch} + P_{k,t,s}^{M,Sell} \quad (75)$$

E) Multi-objective Modeling

After that the cost and emission objective functions were introduced in the previous section, the present section addresses the modeling of a bi-objective problem using two methods of the ε-constraint method and max-min fuzzy method [24].

F) The ε-constraint Method

In the ε-constraint method, one of the objective functions is introduced as the optimization function and the other one as a constraint. The present paper considers the operating cost as the main objective function and pollution emission as the planning constraint. The equations describing the ε-constraint method are given as follows.

$$\Phi_1 = Cost, \Phi_2 = Emission \quad (76)$$

$$OF = \min(\Phi_1) \quad (77)$$

$$\begin{cases} \Phi_2 \le \varepsilon \\ \text{Equal \& Unequal Equations} \end{cases} \quad (78)$$

G) The max-min Fuzzy Method

As shown in Eq. (79), the max-min fuzzy method converts both of the conflicting objective functions into their normalized forms, where $f_k^{\min}$ and $f_k^{\max}$ denote the minimum and maximum values of the objective function k. Also, the optimality level of the *n*th solution of the objective function k is expressed by μ_k^n .

$$\mu_k^n = \begin{cases} 1 & f_k^n \le f_k^{\min} \\ \dfrac{f_k^{\max} - f_k^n}{f_k^{\max} - f_k^{\min}} & f_k^{\min} \le f_k^n \le f_k^{\max} \\ 0 & f_k^n \ge f_k^{\max} \end{cases} \quad (79)$$

After the normalization process, a comparison is made between per unit values of the objective functions in each iteration and the minimum value is selected as given in Eq. (80).

$$\mu^n = \min(\mu_1^n, \cdots, \mu_K^n) \quad (80)$$

The best compromised solution providing a trade-off between two conflicting objective functions is the maximum value of the selected minima (81).

$$\mu^{\max} = \max(\mu^1, \cdots, \mu^N) \quad (81)$$

3. Methodology

The present paper proposes a stochastic two-stage method for configuration and energy management of microgrids in the distribution network. In the first stage, the operation area of each microgrid is determined based on the disconnection from the main grid. In this stage, the structure and protection characteristics of the network are used for forming the microgrids and the main objective is to supply the maximum load possible by available power plants. At the end of this stage, the data of the available equipment in each microgrid is specified considering the service area. These data includes the number of covered points, the capacity of plants, the capacity of the storage system, and the load supplied at each hour. In the second stage, energy management of individual microgrids is carried out independently and the equipment operation mode is determined. In this stage, the microgrid is not operating in the emergency mode and it can exchange power with the main grid. As a result, based on its loading, the microgrid will start planning with the objective of minimizing the cost and emissions. As, in the

second stage, the load of each microgrid is among the restored loads, the shifting-load DRP is used to increase the flexibility of the system. Fig. 2 illustrates the stages of the proposed method.

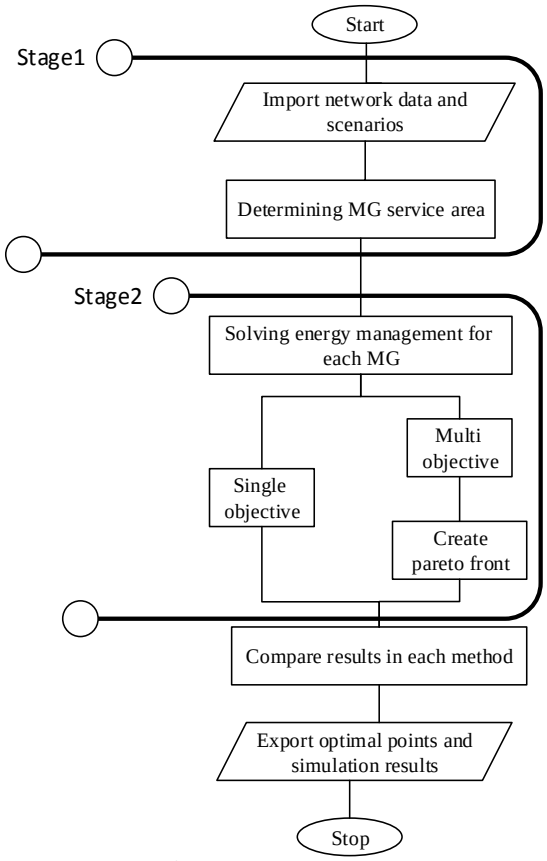

Fig. 2. Flowchart of the proposed method

4. Simulation Results

A) Data

To test the proposed method, a modified 118-bus IEEE distribution network which includes 118 buses, 117 distribution line, and 9 tie lines, is used as a case study [18].The total active and reactive power consumptions of the network under study is 22.71 MW and 17.04 MVAR, respectively. The data required for the place and size of DGs, wind turbines (WTs), and energy storage systems is listed in Table 1. In addition, seven DG units of 14 available DG units can be utilized as the main unit; therefore, the maximum number of formable microgrids is seven. Capacity and efficiency of charging and discharging of the CAES system are assumed 500 kWh and 0.95. Capacity of WTs is considered 500 kW. Table 1 summarizes the system equipment characteristics. It is assumed in this study that for loads greater than 400 kW the load control can be used.

The current research also takes into account the electrical energy consumption level, renewable wind sources generation level, and the price of electricity. The number of scenarios for each of the three mentioned scenarios is 10. Fig. 3 shows the hourly curve for different scenarios.

B) Results of the First Stage

In the performed study on the 118-bus IEEE distribution network, the considered event is flood occurrence. In these situations, a number of nodes and lines of the network are interrupted and as a result, according to the performance of the protection system, part of the system experiences the islanded operation mode. To solve the issue, the proposed method supplies the load with the minimum level of the lost load. In the simulation process, several microgrids that can be implemented under different scenarios and provide the maximum resiliency are formed. The inactive part in Fig. 4 is right side of buses 11, 5, 28, 65, 89 (buses 90-93, 97-99).

Table.1.
Characteristics of the equipment including power plants, the storage system, and renewable wind sources

Distributed generation					***CAES***		***Wind***	
Unit	***Bus no.***	***Cap. (kW)***	***Q^{max} (kVAr)***	***Q^{min} (kVAr)***	***Unit***	***Bus no.***	***Unit***	***Bus no.***
DG1	17	800	600	-600	CAES1	12	WT1	14
DG2	24	1000	800	-800	CAES2	26	WT2	27
DG3	51	900	800	-800	CAES3	40	WT3	42
DG4	59	1200	1000	-1000	CAES4	53	WT4	53
DG5	67	1000	800	-800	CAES5	72	WT5	74
DG6	76	1100	800	-800	CAES6	80	WT6	84
DG7	107	1500	1200	-1200	CAES7	90	WT7	88
DG8	7	200	150	-150	CAES8	110	WT8	96
DG9	33	300	200	-200			WT9	99
DG10	43	300	200	-200			WT10	112
DG11	88	200	100	-100				
DG12	103	500	300	-300				
DG13	113	300	150	-150				
DG14	117	300	150	-150				

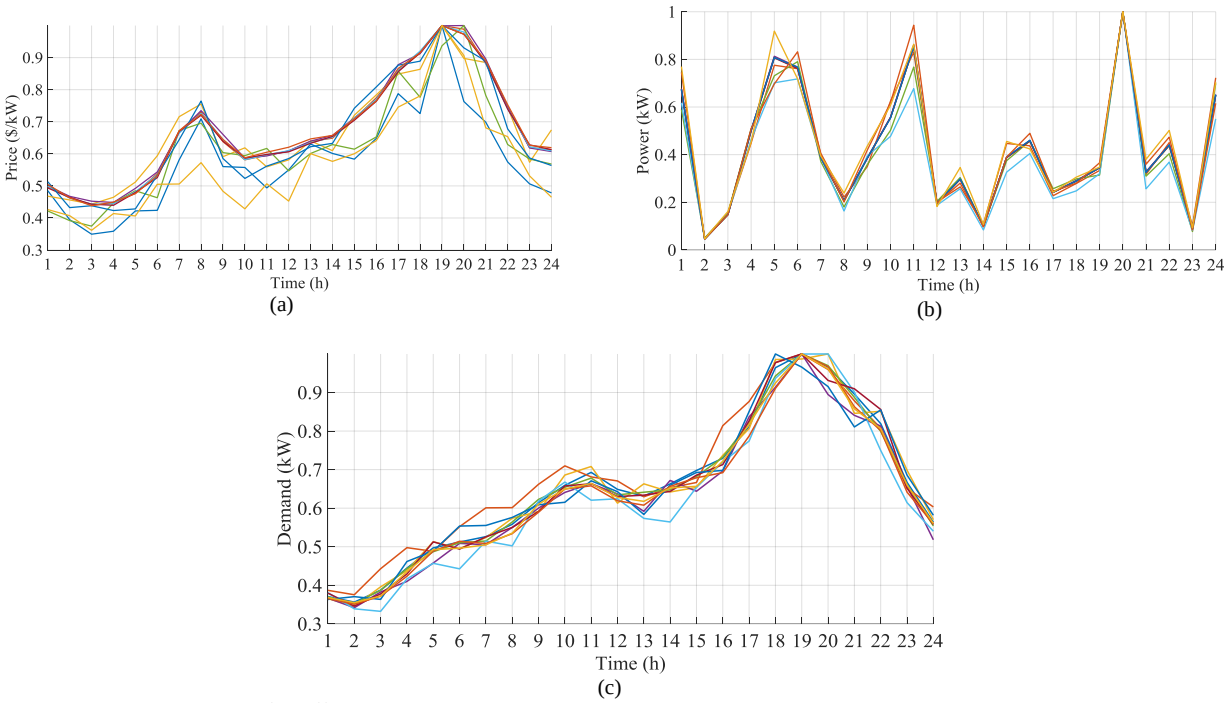

Fig. 3. The hourly curve for different scenarios, (a) price, (b) wind generation, and (c) load

As is observed in Fig. 4, due to the occurrence of flood in feeders 1 and 2, buses of the network located on the path of energizing the main lines, which are equipped with protective switches, have become inactivate. Moreover, as Feeder 3 is healthy, this part of the network correctly operates and is disconnected from the network when the breaker on Line 25 (between nodes 93 and 94) operates and disconnects. This section is shown in green in the figure.

Fig. 5 depicts the configurations of the formed microgrids. According to this figure, two microgrids have been formed within the fault area. Under these conditions, sixty-three buses from 87 faulty buses have been recovered. The active power supplied in this case is 7716.75 kW. Table 2 provides the details of the formed microgrids.

Referring to Table 2 and according to the amount of use of the load control, the load recovery percent in the two microgrids 1 and 2 is 85.67% and 73.22%, respectively. The reason for the higher level of recovery in Microgrid 1 is the larger capacity of the storage system in this microgrid.

To better understand how the load control is used in different points, Fig. 6 indicates the load level before and after the load control actions for the area of each microgrid. It seems that buses 6 and 4 have been used in microgrids 1 and 2, respectively.

C) Results of the Second Stage

Configuration of individual microgrids and the equipment available in their area have been determined in the first stage. In the second stage, the results obtained from solving the energy management problem are described using three different case studies as follows.

- *Case 1*: Single-objective planning,
- *Case 2*: Multi-objective planning using the max-min fuzzy method, and
- *Case 3*: Multi-objective planning using the ε-constraint method.

1) *Case 1*

The planning in Case 1 is carried out to minimize the total cost of the system. In this case, a conversion factor is applied to the amount of pollution in the form of cash penalty to be considered the emission level in the objective function. The operating cost in this case is $51922.88. Also, the emission produced in this case is 46377.31 kg. Fig. 7 shows the hourly curve of power exchange with the main grid. According to Fig. 7, energy purchase at the first hours of the day is greater than that of the peak-load hours. The reasons behind it are energy storage in the battery during these hours because of the low electricity price and the use of a load control program.

Fig. 8 illustrates the level of use of the load control program during different hours. Furthermore, the effect of use of the load control program on the consumption load curve is shown in Fig. 9. Based on the figure, the load control program helps reduce load during peak hours and shift it to off-peak hours of the day.

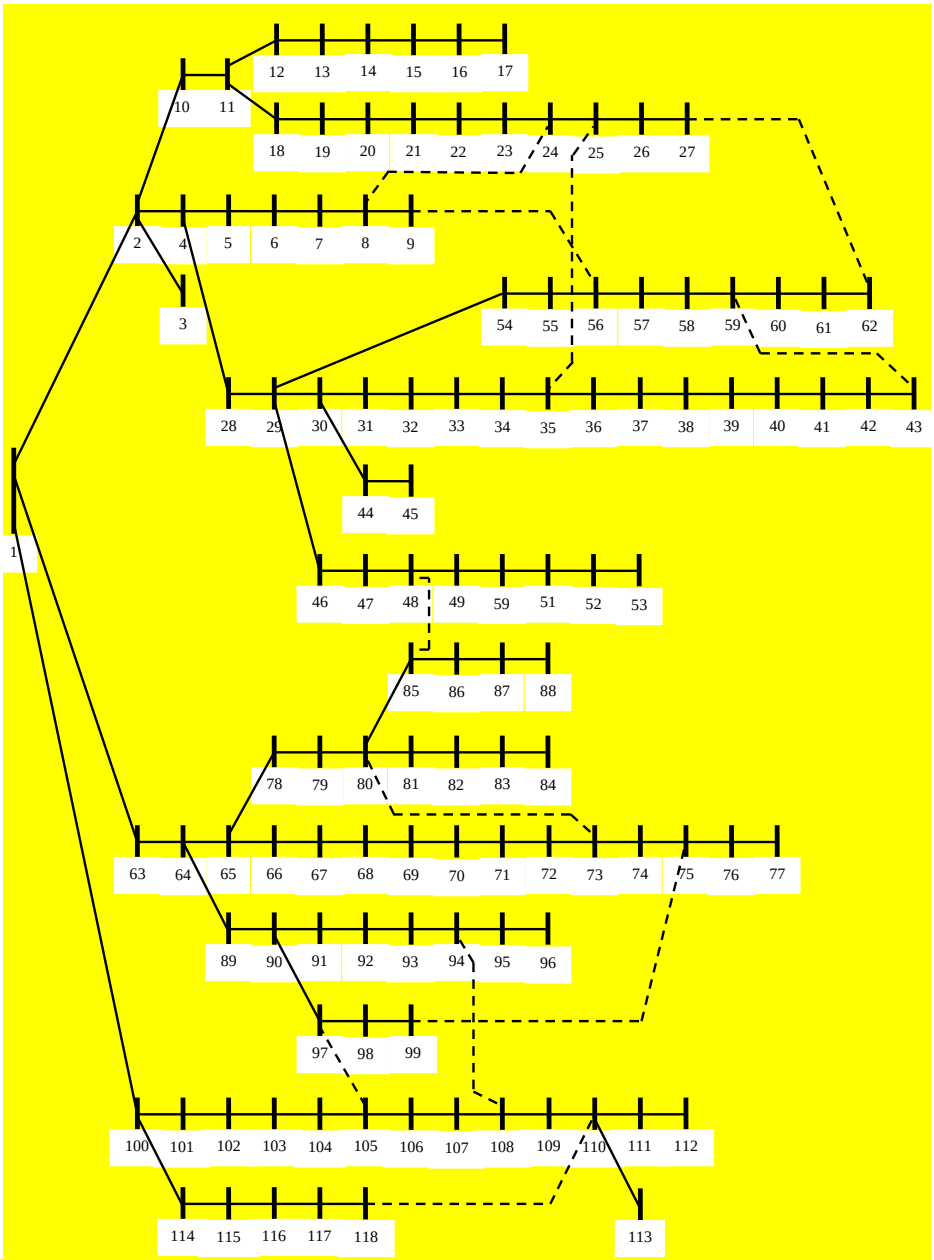

Fig. 4. The system conditions during an event

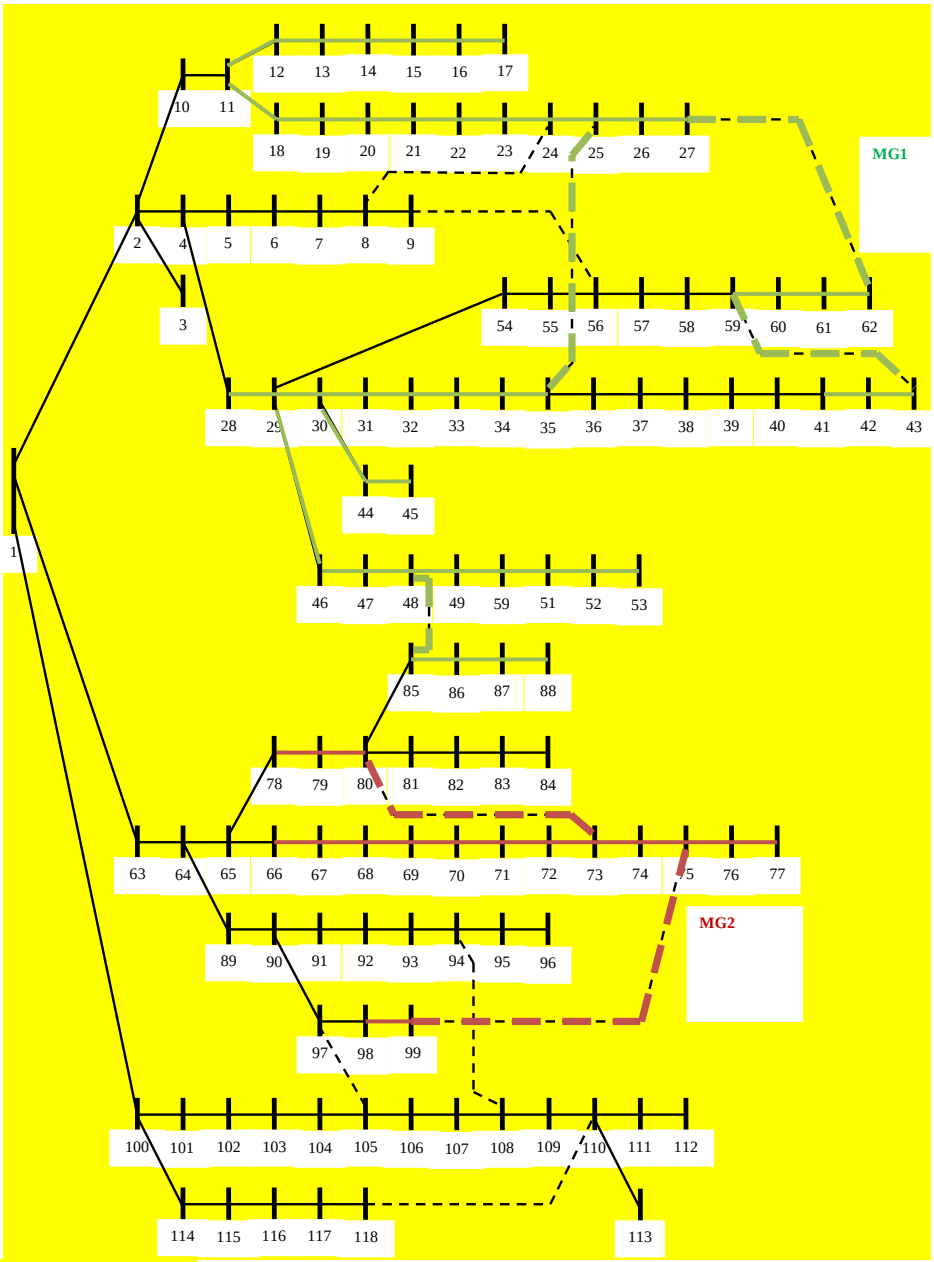

Fig. 5. Area of the formed microgrids

Table.2.
Characteristics of the formed microgrids

MG Number	*Number of covered buses*	*CAES (kW)*	*Wind turbine capacity (kW)*	*Production capacity (kW)*	*Load supplied (kW)*	*Recovery (%)*
MG1	46	1500	2500	4700	5372.44	85.67
MG2	17	1000	1000	2100	2344.31	73.22%

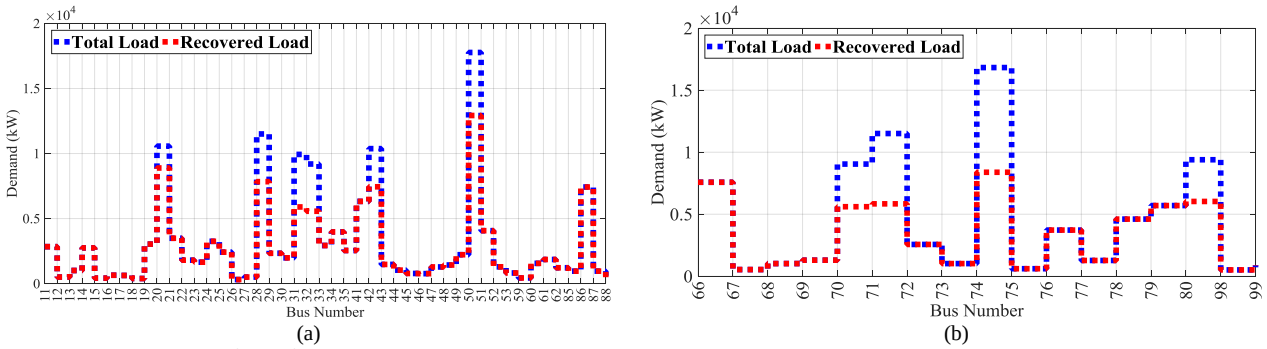

Fig. 6. The level of use of the load control in the network buses, (a) microgrid 1, (b) microgrid 2

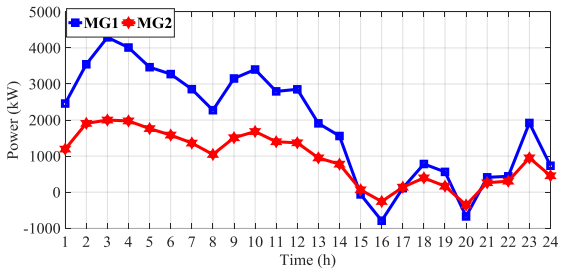

Fig. 7. The hourly curve of power exchange with the main grid

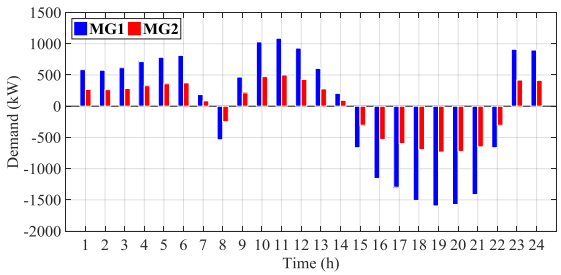

Fig. 8. The level of use of the load control during different hours

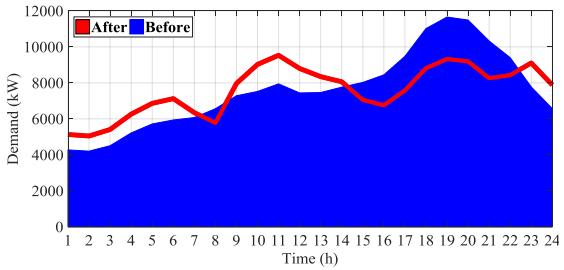

Fig. 9. The hourly load pattern before and after the load control

To study the effect of the load control program as a DRP on the operating cost of each of the microgrids Table 3 presents the results of solving the problem under study with and without the load control program. The results show a significant reduction in the operating cost in the presence of the load control program.

Regarding the use of the CAES system in the model presented in this paper, Fig. 10 depicts the state of charge (SoC) level in the CAES system along with the hourly charging and discharging level for each microgrid.

Fig. 11 shows the amount of gas consumed to supply the power during the peak hours. In these conditions, the storage system reduces the operating cost of the system by storing power in the first hours and injecting power during the peak hours.

With reference to Table 3, it is seen that, in addition to reducing the energy generation and purchase cost, the load control increases the profit obtained from selling energy to the main grid. The operating cost without the load control is $53881.87.

Table.3.
The operation characteristics of the microgrids

		Total Operation Cost ($)	*Generation Cost($)*	*Purchased Electricity($)*	*Sold Electricity($)*	*DRP($)*	*CAES ($)*
With load control	MG1	35356.41	20097.11	14121.97	696.55	416.60	24.18
	MG2	16566.47	9046.04	7012.83	291.75	191.67	24.18
Without load control	MG1	36700.63	21381.91	15240.37	54.17	-	24.18
	MG2	17181.24	9630.39	7526.67	0	-	24.18

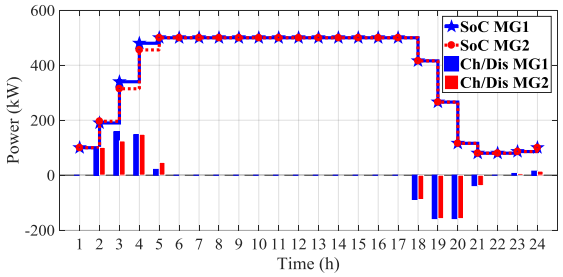

Fig. 10. The state of charge and discharging of the CAES

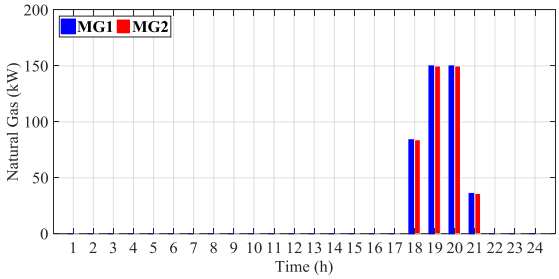

Fig. 11. The purchases gas by the CAES

2) *Cases 2 and 3*

Table 4 tabulates the results obtained for the multi-objective model using the ε-constraint and max-min fuzzy methods. To form Pareto front in both of the mentioned methods and identify the best solution, the fuzzy satisfaction method is employed. The optimal point for each of the method is shown in bold in Table 4. Furthermore, the obtained results from the multi-objective model indicate that the operating cost in the multi-objective case is higher than that in the single-objective case. This is because of modeling the pollution emission as a separate objective function and the reduction in the amount of emissions.

It is inferred from Table 4 that the cost for optimal points of the ε-constraint and max-min fuzzy methods is $52309.46 and $51057.85, respectively. Also, the emission level is 23590.4 kg and 33474.17 kg, respectively. Optimal points besides the Pareto boundary curve for both solution methods are shown in Fig. 12. According to the figure, the operating cost in the ε-constraint is less than that in the fuzzy method. In contrast, the emission level in the latter is less than that in the former.

Table.4.
Results of the multi-objective model

	Fuzzy max-min						*ε-Constraint*				
	Cost	***Emission***	***μ1***	***μ2***	***Max***		***Cost***	***Emission***	***μ1***	***μ2***	***Max***
iter1	58386.65	2460.996	0	0.999	0	iter1	57704.93	2385.546	0.075	1	0.075
iter2	58025.22	2628.659	0.04	0.995	0.04	iter2	55756.19	7686.759	0.289	0.9	0.289
iter3	57898.32	8257.17	0.054	0.889	0.054	iter3	54417.05	12987.97	0.436	0.8	0.436
iter4	58276.84	2907.161	0.012	0.99	0.012	iter4	53317.88	18289.18	0.557	0.7	0.557
iter5	57679.06	3998.856	0.078	0.97	0.078	iter5	**52309.46**	**23590.4**	**0.668**	**0.6**	**0.6**
iter6	54654.1	14000.19	0.41	0.781	0.41	iter6	51372.56	28891.61	0.77	0.5	0.5
iter7	**52104.85**	**27334.17**	**0.689**	**0.529**	**0.689**	iter7	50579.72	34192.82	0.858	0.4	0.4
iter8	50440.41	38303.11	0.873	0.322	0.322	iter8	49995.64	39494.03	0.922	0.3	0.3
iter9	49778.75	45674.3	0.945	0.183	0.183	iter9	49597.07	44795.24	0.965	0.2	0.2
iter10	49619.62	48802.83	0.963	0.124	0.124	iter10	49361.18	50096.46	0.991	0.1	0.1
iter11	49671.77	51652.31	0.957	0.071	0.071	iter11	49282.51	55397.67	1	0	1

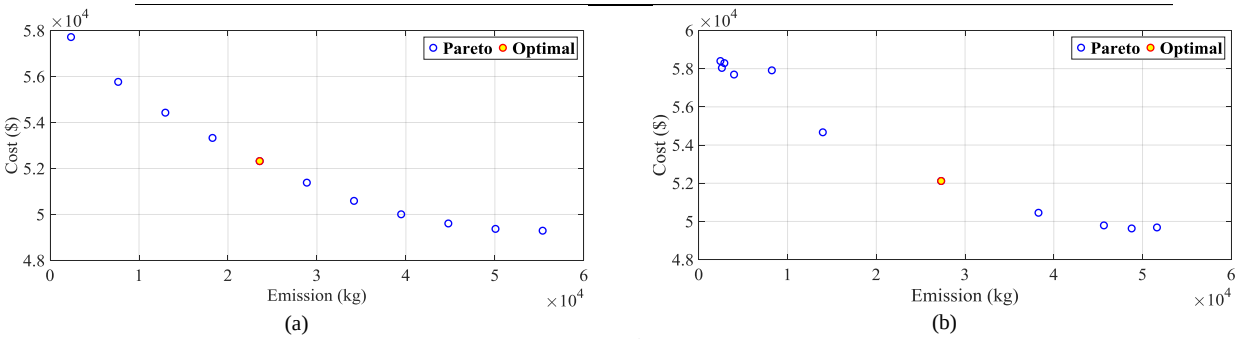

Fig. 12. Pareto boundary, (a) ε-constraint method, and (b) max-min fuzzy method

5. Conclusion

This paper studies the microgrids' operation problem by considering their service area in the form of a two-stage stochastic model. To make the operation conditions close to the real conditions, the uncertainty of planning parameters including the generation power by renewable wind source, the amount of consumption load, and the price have been taken into account in the operation problem. In the first stage, the problem is solved for both grid-connected and islanded operation modes to determine the operation area of each microgrid considering the constraint of maximum resiliency. The results show the accurate determination of the operation area of each microgrid due to considering the security constraints of the network. In the second stage, the microgrids' operation problem is

solved as single-objective and multi-objective problems separately, where the operating cost and emission level are assumed as objective functions. Based on the obtained results, the operating cost is increased in the multi-objective case because of the reduction in the emission level. It should be noted that the multi-objective model proposed in this paper is solved separately using the max-min fuzzy and ε-constraint methods. A comparison between the results of these two methods shows that the operating cost in the latter method is smaller. In contrast, the emission level of the fuzzy method is less than the other method. Additionally, a shiftable load DRP is used in the suggested model. The investigations on the results show the improvement in the demand curve and reduction in the operating cost.

Nomenclature

A) Sets

t	Planning periods
i	Network buses
l	Network lines
s	Scenarios
k	Number of microgrids (MGs)
d	Different degrees of load shedding
g	Distributed generations (DGs)
es	Energy storage systems
w	Wind system

B) Parameters

Pr^L	Load importance factor
ρ	Probability of occurrence of the scenario
φ	Load power factor
P^{Curt}	Maximum capacity of load shedding
$P^{LC.Max}$	Maximum use of load control
P^{Load}/Q^{Load}	Predicted active/reactive load
$P^{DG.Min}$ /$P^{DG.Max}$	Minimum/maximum active power producible by DGs
$Q^{DG.Min}$ /$Q^{DG.Max}$	Minimum/maximum reactive power producible by DGs
$A^{Inject.Min}$/ $A^{Inject.Max}$	Minimum/maximum pressure increase in the reservoir air pressure
$A^{Pump.Min}$/ $A^{Pump.Max}$	Minimum/maximum pressure decrease in the reservoir air pressure
dt	Planning time step
PS^{Min}/ PS^{Max}	Minimum/maximum pressure level in the reservoir air pressure
P^{Wind}	Predicted wind power
v	Wind speed
v_{ci}/v_{co}	Minimum/maximum operating speed of the wind turbine
v_r	Nominal speed of the wind turbine
P_r	Nominal power of the wind turbine
k^1/k^2	Numerical coefficients indicating the line conductance and susceptance
r/x	Line resistance and reactance
$P^{Flow.Max}$ /$Q^{Flow.Max}$	Maximum active/reactive power transferrable on the lines
$a.b.c$	Cost function coefficients of DGs
$\alpha.\beta.\gamma$	Pollution function coefficients of DGs
λ^{EM}	Pollution cost coefficient
$P^{M.Max}$	Maximum power exchange with the main grid
ρ^{Power}	Price of power exchange with the main grid
α^{HR}	Operation coefficient of the compressed-air reservoir under discharge conditions
ρ^{Gas}	Gas price
$EM^{Net.Gas}$	Gas pollution coefficient of the network
$a^{LC}.b^{LC}$	Cost coefficients of the use of load control

C) Variables

P^L/Q^L	The amount of supplied active/reactive demand
α	Active/inactive status of the bus
B	Active/inactive status of the line
χ/χ'	Auxiliary variables that determine the active/inactive status of the line
P^{LC}	The level of use of load control
σ^{LC}	A binary variable showing the capacity of load shedding
P^{DG} /Q^{DG}	Active/reactive power generated by DGs
A^{Inject}	Increased pressure level under air reservoir discharge
A^{Pump}	Decreased pressure level under air reservoir discharge
P^{Ch}	Power consumption by the air reservoir under discharge conditions
P^{Dch}	Power supply by the air reservoir under discharge conditions
I^{Ch}/I^{Dch}	A binary variable determining the charge/discharge status
PS	Air pressure level of the reservoir
P^{Flow} /Q^{Flow}	Active/reactive power flow on the lines
V	Bus voltage amplitude
δ	Bus voltage angle
P^{DG2}	Quadratic value of active power generation by DGs
$C^{SU}.C^{SD}$	Startup/shutdown cost of DGs
$u^{SU}.u^{SD}$	A binary variable showing the startup/shutdown status of DGs
C^{LC}	The cost of use of load control
C^M	The cost of power exchange with the

	main grid
C^{ES}	The cost of use of storage devices
E^{ES}	Pollution caused by storage devices
P^{M}	Power exchanged with the main grid
$P^{M.sell}$	Power sell to the main grid
$P^{M.buy}$	Power purchase from the main grid
u^{sell} /u^{buy}	A binary variable showing the energy sell/purchase status
P^{Gas}	Gas consumption level under reservoir discharge conditions
$P^{LC.Up}$/ $P^{LC.Do}$	Load increase/decrease during the use of load control
I^{Up}/I^{Do}	A binary variable showing the status of use of increased/decreased load control

References

[1] Panteli, M., and et al., "Metrics and Quantification of Operational and Infrastructure Resilience in Power Systems," 2017, *IEEE Trans. Power Syst.*, vol. 32, no. 6, pp. 4732–4742.

[2] Shahidehpour, M., liu, x., Li, Z., and Cao, Y., "Microgrids for Enhancing the Power Grid Resilience in Extreme Conditions," 2016, *IEEE Trans. Smart Grid*, p. 1.

[3] Ton, D. T. and Wang, W.-T. P., "A More Resilient Grid: The U.S. Department of Energy Joins with Stakeholders in an R&D Plan," 2015, *IEEE Power and Energy Mag.*, vol. 13, no. 3, pp. 26–34.

[4] Jimenez-Estevez, G., and et al., "Achieving Resilience at Distribution Level: Learning from Isolated Community Microgrids," 2017, *IEEE Power and Energy Mag.*, vol. 15, no. 3, pp. 64–73.

[5] Li, Z., Shahidehpour, M., Aminifar, F., Alabdulwahab, A., and Al-Turki, Y., "Networked Microgrids for Enhancing the Power System Resilience," 2017, *Proc. IEEE*, vol. 105, no. 7, pp. 1289–1310.

[6] Bie, Z., Lin, Y., Li, G., and Li, F., "Battling the Extreme: A Study on the Power System Resilience," 2017, *Proc. IEEE*, vol. 105, no. 7, pp. 1253–1266.

[7] Chen, C., Wang, J., and Ton, D., "Modernizing Distribution System Restoration to Achieve Grid Resiliency Against Extreme Weather Events: An Integrated Solution," 2017, *Proc. IEEE*, vol. 105, no. 7, pp. 1267–1288.

[8] Chanda, S. and Srivastava, A. K., "Defining and Enabling Resiliency of Electric Distribution Systems With Multiple Microgrids," 2016, *IEEE Trans. Smart Grid*, vol. 7, no. 6, pp. 2859–2868.

[9] Bajpai, P., Chanda, S., and Srivastava, A. K., "A Novel Metric to Quantify and Enable Resilient Distribution System Using Graph Theory and Choquet Integral," 2018, *IEEE Trans. Smart Grid*, vol. 9, no. 4, pp. 2918–2929.

[10] Gao, H., Chen, Y., Xu, Y., and Liu, C.-C., "Resilience-Oriented Critical Load Restoration Using Microgrids in Distribution Systems," 2016, *IEEE Trans. Smart Grid*, vol. 7, no. 6, pp. 2837–2848.

[11] El-Sharafy, M. Z. and Farag, H. E., "Back-feed power restoration using distributed constraint optimization in smart distribution grids clustered into microgrids," 2017, *Applied energy*, vol. 206, pp. 1102–1117.

[12] Craparo, E., Karatas, M., and Singham, D. I., "A robust optimization approach to hybrid microgrid operation using ensemble weather forecasts," 2017, *Applied energy*, vol. 201, pp. 135–147.

[13] Farzin, H., Fotuhi-Firuzabad, M., and Moeini-Aghtaie, M., "Enhancing Power System Resilience Through Hierarchical Outage Management in Multi-Microgrids," 2016, *IEEE Trans. Smart Grid*, vol. 7, no. 6, pp. 2869–2879.

[14] Haddadian, H. and Noroozian, R., "Multi-microgrids approach for design and operation of future distribution networks based on novel technical indices," 2017, *Applied energy*, vol. 185, pp. 650–663.

[15] Nikmehr, N., Najafi-Ravadanegh, S., and Khodaei, A., "Probabilistic optimal scheduling of networked microgrids considering time-based demand response programs under uncertainty," 2017, *Applied energy*, vol. 198, pp. 267–279.

[16] Mazidi, M., Monsef, H., and Siano, P., "Robust day-ahead scheduling of smart distribution networks considering demand response programs," 2016, *Applied energy*, vol. 178, pp. 929–942.

[17] Daneshvar, M., Mohammadi-Ivatloo, B., Asadi, S., Zare, K., and Anvari-Moghaddam, A., "Optimal Day-Ahead Scheduling of the Renewable Based Energy Hubs Considering Demand Side Energy Management," In *2019 International Conference on Smart Energy Systems and Technologies (SEST)*, 1–6.

[18] Mousavizadeh, S., Haghifam, M.-R., and Shariatkhah, M.-H., "A linear two-stage method for resiliency analysis in distribution systems considering renewable energy and demand response resources," 2018, *Applied energy*, vol. 211, pp. 443–460.

[19] Wang, D., Qiu, J., Reedman, L., Meng, K., and Lai, L. L., "Two-stage energy management for networked microgrids with high renewable penetration," 2018, *Applied energy*, vol. 226, pp. 39–48.

[20] Li, Y., Wang, J., Han, Y., Zhao, Q., Fang, X., and Cao, Z., "Robust and opportunistic scheduling of district integrated natural gas and power system with high wind power penetration considering demand flexibility and compressed air energy storage," 2020, *Journal of Cleaner Production*, vol. 256, p. 120456.

[21] Govardhan, M. and Roy, R., "Generation scheduling in smart grid environment using global best artificial bee colony algorithm," 2015, *International Journal of Electrical Power & Energy Systems*, vol. 64, pp. 260–274.

[22] Yuan, H., Li, F., Wei, Y., and Zhu, J., "Novel Linearized Power Flow and Linearized OPF Models for Active Distribution Networks With Application in Distribution LMP," 2018, *IEEE Trans. Smart Grid*, vol. 9, no. 1, pp. 438–448.

[23] Liang, H., Liu, Y., Li, F., and Shen, Y., "A multiobjective hybrid bat algorithm for combined economic/emission dispatch," 2018, *International Journal of Electrical Power & Energy Systems*, vol. 101, pp. 103–115.

[24] Lin, J. and Wang, Z.-J., "Multi-area economic dispatch using an improved stochastic fractal search algorithm," 2019, *Energy*, vol. 166, pp. 47–58.